ISSN: 2160-049X Volume 9, Number 6, June 2019

Scientific Research Publishing

World Journal of Mechanics

ISSN: 2160-049X
9 772160 049007 06

www.scirp.org/journal/wjm

Journal Editorial Board

ISSN 2160-049X (Print) ISSN 2160-0503 (Online)

http://www.scirp.org/journal/wjm

Editors-in-Chief

Scientific Research Publishing

World Journal of Mechanics, 2019, 9, 147-176
http://www.scirp.org/journal/wjm
ISSN Online: 2160-0503
ISSN Print: 2160-049X

Table of Contents

Volume 9 Number 6 June 2019

World Journal of Mechanics (WJM)
Journal Information

SUBSCRIPTIONS

The *World Journal of Mechanics* (Online at Scientific Research Publishing, www.SciRP.org) is published monthly by Scientific Research Publishing, Inc., USA.

Subscription rates:
Print: $69 per issue.
To subscribe, please contact Journals Subscriptions Department, E-mail: sub@scirp.org

SERVICES

Advertisements
Advertisement Sales Department, E-mail: service@scirp.org

Reprints (minimum quantity 100 copies)
Reprints Co-ordinator, Scientific Research Publishing, Inc., USA.
E-mail: sub@scirp.org

COPYRIGHT

PRODUCTION INFORMATION

For manuscripts that have been accepted for publication, please contact:
E-mail: wjm@scirp.org

Scientific Research Publishing

World Journal of Mechanics, 2019, 9, 147-162
http://www.scirp.org/journal/wjm
ISSN Online: 2160-0503
ISSN Print: 2160-049X

Improvement of Interlaminar Fracture Properties of Out of Autoclave Manufactured Carbon Fiber Reinforced Polymers Using Multi-Walled Carbon Nanotubes

Dimoka Polyxeni[1], Kostagiannakopoulou Christina[1], Masouras Athanasios[1], Kostopoulos Vassilis[1,2*]

[1]Department of Mechanical Engineering and Aeronautics, University of Patras, Patras, Greece
[2]Institute of Chemical Engineering Sciences, Foundation for Research and Technology Hellas (ICE-HT/FORTH), Patras, Greece
Email: dimoka@mech.upatras.gr, kostagia@mech.upatras.gr, atmas@mech.upatras.gr, *kostopoulos@mech.upatras.gr

How to cite this paper: Polyxeni, D., Christina, K., Athanasios, M. and Vassilis, K. (2019) Improvement of Interlaminar Fracture Properties of Out of Autoclave Manufactured Carbon Fiber Reinforced Polymers Using Multi-Walled Carbon Nanotubes. *World Journal of Mechanics*, **9**, 147-162.
https://doi.org/10.4236/wjm.2019.96010

Received: March 6, 2019
Accepted: May 26, 2019
Published: May 29, 2019

Abstract

The present study aims to the development of Out of Autoclave (OoA) Carbon Fiber Reinforced Polymers (CFRPs) with increased interlaminar fracture toughness by using MWCNTs. The introduction of MWCNTs into the structure of CFRPs has been succeeded by using carbon nanotube-enriched sizing agent for the pretreatment of the fiber preform using an in-house developed methodology that can be easily scaled up. The positive effect of the proposed methodology on the interlaminar fracture toughness of the CFRP laminate was assessed by the increase of Mode I and Mode II interlaminar fracture toughness of the composites. Different wt% MWCNTs concentrations were used (namely 0.5%, 1%, 1.5% and 2.5%). It was found that the nanomodified composites exhibit a significant increase of the interlaminar critical strain energy release rate G_{IC} and G_{IIC} of the order of 103% and 62% respectively, in the case of 1.5 wt% MWCNTs weight content. Scanning Electron Microscopy (SEM) of the fracture surfaces of CFRP samples revealed the contribution and the associated synergistic mechanisms of MWCNTs to the increase of the crack propagation resistance in the case of nano-modified CFRPs compared to the reference material.

Keywords

Multi-Walled Carbon Nanotubes (MWCNTs), Interlaminar Fracture Toughness, Multi-Scale Composites (CFRPs), Out of Autoclave (OoA)

1. Introduction

Carbon Fiber Reinforced Polymers (CFRPs) are increasingly used as advanced structural materials in various fields of applications such as aerospace, automotive, sports, energy and military industries. This tendency is clearly driven by their high specific strength and stiffness as well as their corrosion resistance compared to the conventional metals. Carbon fibers (CFs) are the most ideal reinforcement candidates because of their attractive properties such as high strength and modulus, high electrical conductivity, high thermal conductivity and low density. On the other hand, epoxy resins are the mostly used thermosetting matrices in FRPs due to their good mechanical properties, excellent corrosion resistance, high thermal stability and high compatibility with carbon, glass and aramid fiber reinforcements. However, poor out-of-plane properties of composites are observed due to the absence of the through-thickness reinforcement in order to sustain transverse loads.

Therefore, the weak fiber-matrix interface and the brittle nature of epoxy matrix in composite laminates make them prompt to interlaminar failures, such as delamination. Hence, it is imperative to find an effective way to satisfy multifunctional requirements and through-thickness reinforcements without compromising the in-plane properties. To this direction, there have been a number of attempts where many researchers have successfully developed through the thickness reinforcement methods to improve the fracture toughness of FRPs by using different methods, such as z-pinning [1] [2] [3], 3-D weaving, stitching [4] [5] [6] knitting, interleaving and toughening the matrix using micro-phase particles including rubbery or thermoplastics polymers [7]. However, the major disadvantage of these approaches is the development of large resin rich areas within the composite structure and therefore the deterioration of their in-plane properties. In view of this, a new field of research has been evolved improving the thermosetting matrices with the incorporation of nano-sized fillers [8] [9] [10]. The nano-phase introduces additional energy dissipation mechanisms during failure and therefore contributes to the improvement of interlaminar fracture toughness of the composite. Thus, the multi-scale reinforcement approach has resulted in the enhancement of damage tolerance and multi-functionality of conventional composites.

Towards this direction, Multi Wall Carbon Nanotubes (MWCNTs) is highly potential filler due to the superior mechanical, electrical and thermal properties [11]. Furthermore, their high aspect ratio and specific surface area provides a solid background for increasing the fracture characteristics of a resin system, where MWCNTs have been homogeneously dispersed [12] [13] [14] [15]. In the case of nano-modified with MWCNTs epoxy matrix, which has been used for composite manufacturing, then a significant increase of the interlaminar fracture toughness has been reported by Kostopoulos *et al.* [12]. More precisely, in the case where 1%wt. MWCNTs has been homogeneously dispersed into the epoxy matrix the interlaminar fracture toughness G_{IC} and G_{IIC} of the composite was in-

creased by 60% and 75% respectively. Gojny *et al.* has demonstrated an increase of fracture toughness of epoxy resin by 23%, in the case 1wt% amino-functionalized Double Wall CNTs has been homogeneously dispersed into the epoxy via three roll calander [16]. Davis *et al.* in [17] demonstrated that fluorine functionalized carbon nanotubes (f-CNTs) can be used in the midplane of a fiber reinforced epoxy composite laminate for increasing the Mode II interlaminar fracture toughness. The highest improvement of 27% in the average propagation G_{IIC} was observed with 0.5 wt% f-CNTs.

Although the introduction of CNTs into composite laminates provide significant performance benefits dealing mainly with the interlaminar fracture characteristics and the resulted multi-functionality, many problems appear during the incorporation of CNTs into these materials, especially in the OoA manufacturing processes. A direct introduction of CNTs into epoxy matrix leads to increase of resin viscosity and an uneven nanofiller distribution into the manufactured component and/or filtering effects that block the resin close to the inlet gates. This difficulty makes almost impossible the direct introduction of CNTs during Out-of-Autoclave (OoA) processes such as resin infusion or resin transfer molding (RTM). Despite this problem, many attempts have been made to infuse nano-modified epoxy resin through the fiber preform for enhancing out-of-plane properties and are based on the significant decrease on the amount of CNTs into the resin and their functionalization to minimize agglomerates. More precisely, Zhou *et al.* [18] proposed the implementation of nanocomposites with 0.3 wt% CNTs by VARTM method and an improvement of 2% in flexural strength was reported. They found that MWCNT/epoxy suspension higher than 0.5 wt% could not penetrate the fabrics preform thus blocking the resin flow. Advani *et al.* [19] has studied the filtering effect of acid-oxidized MWCNTs on the fabric surface. Zhang *et al.* [20] reported the increase of 14% in tensile strength and 20% in modulus by infusing 1%wt. loading of functionalized MWCNTs into glass fabrics. Regarding the interlaminar fracture toughness, Tanoglu *et al.* [21] observed an enhancement of 8% in G_{IIC} with 0.1% wt. amino functionalized CNTs composites whereas no significant improvement for G_{IC} value was reported. K.T. Hsiao *et al.* [22] introduced CNFs into polyester matrix to manufacture a multiscale glass fiber reinforced composites by resin infusion process at various concentrations (0.5, 1, 1.5 wt%). In the case of 1.5 wt% noticeable CNF filtration effect in the thickness direction was shown and the presence of micro-void formation in the specimens was observed.

Due to the existence of the resin filtering problem in VARTM processes, several studies have focused on the developing of a hybridization method for the introduction of CNT/CF into the final OoA product. The chemical vapor deposition (CVD) and chemically grafting methods to grow directly CNTs on the carbon fabric surface, are effective techniques for improving the interfacial bonding between fiber and matrix [23] [24] [25] [26]. The CVD approach, however, can cause a reduction in the strength of the carbon fibers due to the extreme conditions (high operational temperature over 700˚C and large time of

process stabilization) [27] and, therefore, compromise the tensile properties. Additionally, in light of this issue, many attempts have developed in order to well vertically align the carbon nanotubes on the carbon fiber surface [28]. Furthermore, this technique is difficult to implement on an industrial scale. As an alternate method, the spraying technique and electrophoretic deposition (EPD) of CNT fillers are industrial-coating and low-energy use techniques that offer the capacity of homogeneous coating of complex shapes with well adhered films of controlled thickness, thus improving out-of-plane properties such as interlaminar fracture toughness in case they are applied in each layer of the fiber preform. For the implementation of spraying technique, an airbrush system is used to spray the CNTs solution onto the fabric surface and then the solvent is removed remaining the CNTs-modified fabrics [29].

The objective of the present study is the introduction of the CNTs in to the fiber preform through an alternative methodology that includes its modification by the integration of MWCNTs in a form of CNTs-enriched sizing agent. A water-based solution with a given wt% CNTs content was prepared and the carbon fiber woven reinforcement was passed through it at a given rate. Then the fabric was dried, and the dry fabric used to prepare the fiber preform and the final preform was placed in to the mold. Then all preparation for steps for the application of OoA process was applied. During the nano-modification treatment of the woven fabric up to the application of infusion process all the steps have been performed in a closed hood equipped with the appropriate nano-filter under slight under-pressure. After the manufacturing of the CNT modified plates the effect on the influence of MWCNTs on the interlaminar fracture toughness of CFRPs was assessed. The goal of this work is to study the ability of MWCNTs to provide increased resistance against interlaminar cracking and delamination. In this work, five CFRP laminated plates were manufactured using liquid resin infusion (LRI) process, with different weight content of CNTs (0, 0.5, 1, 1.5 and 2.5 wt%). Mode I and Mode II tests were carried out and the fracture energy as a function of the MWCNT content was measured. Finally, energy dissipation mechanisms, where the nano fillers contribute, were demonstrated by detail observation of fracture surfaces using scanning electron microscope (SEM).

2. Manufacturing Processes

2.1. Materials

The matrix material used in this study was a three-part epoxy system provided by Resoltech Advanced Technology Resin (France). This resin system consists of an epoxy resin (Resolcoat 1400), an anhydride hardener (Resolcoat 1407) and an imidazole accelerator (AC140), which are typically mixed in ratios of 100:90:0.5 by weight, as recommended by the manufacturer [30]. The hardener and the accelerator were premixed, and the epoxy resin was preheated at 40˚C before adding the cold hardener. The resulting epoxy system has a low viscosity, good mechanical adhesion and is very versatile for fabricating composite parts using re-

sin transfer molding technique.

The main reinforcement phase was a twill weave carbon fabric with a density per unit area of 194 g/m^2, having 3 K filaments in the fiber bundle and a dry ply thickness of approximately 0.35 mm. The carbon fabric reinforcement (having fiber type TR30S) was supplied by Fibermax Composites (Greece). The Pyrofil TR30S fiber type is a high strength and high modulus aerospace fiber with a reported tensile strength up to 4410 MPa, an elastic modulus close to 235 GPa and density of 1.79 g/cm^3 [31].

Regarding the nano-phase, a liquid CNT-enriched sizing agent (SIZICYL XC R2G) was purchased from Nanocyl SA, Belgium. It is a sizing agent modified with 6.2% maximum solid content of MWCNTs (NC7000, Nanocyl) to size fabrics before impregnation by the resin matrix [32]. It has excellent compatibility with glass and carbon fibers to improve mechanical properties of a composite structure, without affecting the viscosity of the resin used to impregnate the fiber.

2.2. Preparation of MWCNTs Suspension

The MWCNT-enriched sizing agent solution was prepared by mixing an amount of sizing agent into a suitable quantity of distilled water, obtaining a water solution with certain content of CNTs. Different solutions with different CNT content was used for the pretreatment of the carbon fabric to conclude to different CNTs wt% content. Then, ultrasonic processing with a tip sonication device (Bandelin) was employed to homogeneous disperse the MWCNTs in the suspension for 3 h, operated at an output power of 60 W. To avoid temperature increases in the bulk solution during ultrasonication, the mixing pot was placed into a temperature control bath with continuous feed of fresh water. The quality control of the mixture was performed using a grindometer to confirm the absence of agglomerates. Finally, prior to pretreatment of carbon fabric reinforcement, the prepared water-based solution was degassed in a vacuum chamber for about 5 min.

2.3. Nano-Reinforced CFRP Laminates

Composite plates with various CNTs concentrations (0, 0.5, 1, 1.5 and 2.5 wt%) were manufactured using an in-house developed process. Carbon fiber reinforced composite laminated plates (CFRPs) of 200 × 300 mm^2 were produced by Vacuum Assisted Resin Infusion process (VARI).

The prepared water based MWCNTs suspension, described earlier was used for the nano-modification of dry carbon fabrics in a closed hood equipped with the appropriate nano-filters under slight under-pressure. The fabric reinforcement was passed through the solution at a given rate and slightly compressed at the output of the solution bath. Then, the nano-modified wet fabrics were left to dry using a thermal plate. To calculate the final amount of MWCNTs deposited/infiltrated in the carbon fabrics, the mass of a given carbon fabric surface was measured before and after deposition.

Each laminate was composed of sixteen carbon fabric layers and a 13 μm thick PTFE (polytetrafluoroethylene) film of 70 mm wide and 250 mm long was placed in the middle plane (between 8th and 9th ply) of each plate to generate the starter crack, which is required to perform the interlaminar fracture tests. In the case of nano-doped laminates, four nano-modified CF layers for each filler content were placed in the middle of the laminates. Then, the carbon fabrics of each laminate were stacked on a mold, covered by a highly permeable medium and sealed with vacuum bag. The epoxy resin was infused through the fabrics and the laminates were cured in a conventional oven at 80˚C for 4 h followed by post-cure profile at 140˚C for 4 h according to manufacturer instructions. The step by step preparation of doped CFRP laminates is schematically depicted in Figure 1. Reference and unmodified CFRP plates, were also manufactured. The thickness and the fiber volume fraction of all produced plates were measured around 3.1 mm and 58% respectively, while the exact figures are shown in Table 1. Ultrasonic inspection was carried out utilizing the C-scan equipment (pulse-eco technique with 5 kHz transducer) and the results showed very good and fully acceptable quality of the manufactured plates, without major defects (thickness variations, inhomogeneities and porosity).

2.4. Mode I and Mode II Fracture Tests

The resistance to interlaminar crack propagation of the produced laminates was defined by performing two types of fracture toughness experiments both for reference and MWCNT-modified specimens to quantify the interlaminar toughening effect resulted by the nano-modification of woven fabric with MWCNTs. A hydraulic universal testing machine (Instron, 8872) equipped with a 25kN loadcell was used for Mode I and Mode II tests. Five samples were tested for each type of material and for each type of experiment. The energy release rate under Mode I (G_{IC}) was determined by using the double cantilever beam (DCB) method and was carried out according to ASTM standard D5528 [33]. DCB specimens were cut with the length of 250 mm, width of 25mm and an initial crack length of 25 mm. Crack propagation was visually observed from the specimens marked side surface using a CCD camera equipped with a magnification lens (×10). The crosshead speed used was 5 mm/min.

Table 1. Thickness and fiber volume fraction of produced laminates.

Laminate	MWCNTs content (wt%)	Thickness (mm)	Fiber volume fraction V_f (%)
Plate 1-Ref.	0	3.06 ± 0.02	58
Plate 2-P05	0.5	3.13 ± 0.03	57
Plate 3-P10	1	3.11 ± 0.06	58
Plate 4-P15	1.5	3.07 ± 0.03	58
Plate 5-P25	2.5	3.2 ± 0.02	55

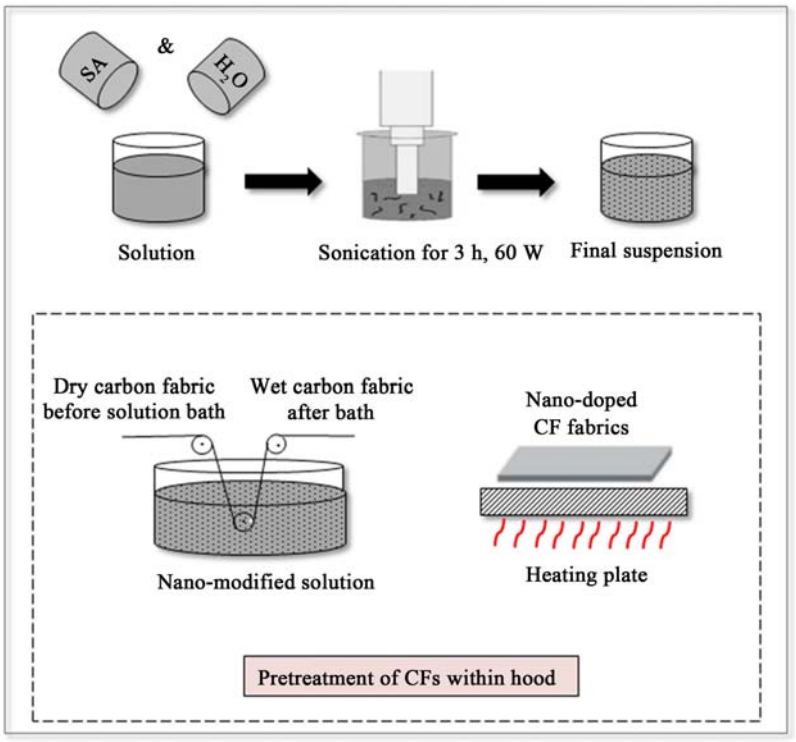

(a)

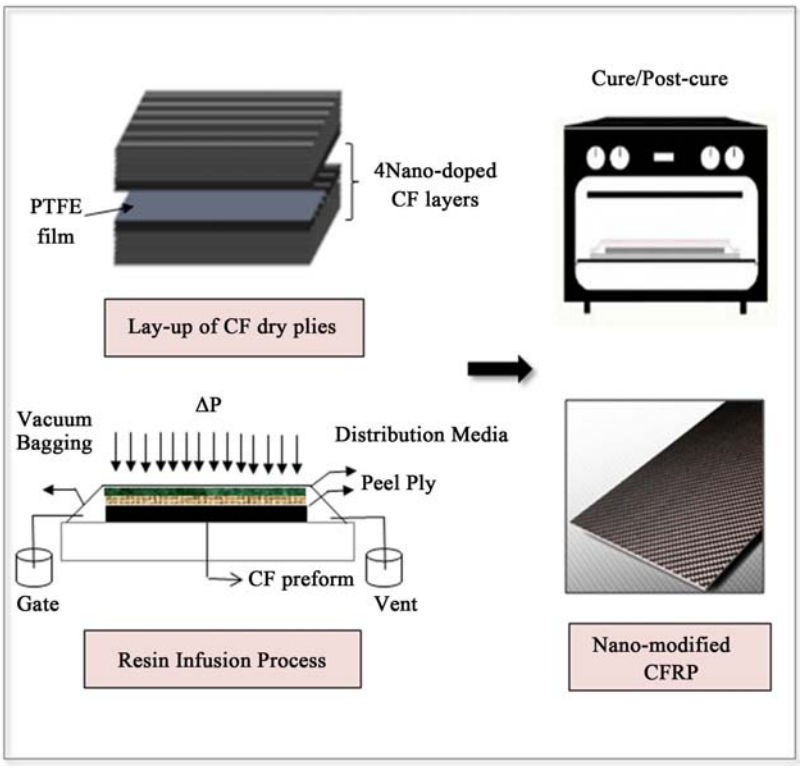

(b)

Figure 1. Illustration ofstep by step preparation process of nano-modified CFRP laminates. (a) The pretreatment process of dry carbon fiber to produce nano-modified reinforcement; and (b) The manufacturing production of CFRP laminates using infusion process.

The Mode II interlaminar fracture toughness (G_{IIC}) was measured by using the three-point end notched-flexure (3ENF) method in accordance to ASTM D7905 [34]. The test specimens were 120 mm long with the nominal specimen span length (2 L) of 100 mm and a nominal half-span length (L) of 50 mm. (The nominal thickness of the samples used in mode II tests is slightly smaller to the one suggested by the standard *i.e.* 3.1 mm instead of 3.38 mm). The crosshead speed was kept at 1 mm/min. Finally, the fracture surfaces of tested specimens were examined using a FEI InspectTM F50 Scanning Electron Microscopy (SEM).

3. Results and Discussion

3.1. Mode I DCB Tests

Typical load-displacement curves of DCB specimens for the reference and nano-doped laminates are displayed in **Figure 2(a)**. Both the reference and nano-doped laminates show a linear load-displacement relationship up to the point of the crack initiation, after which they demonstrate distinct crack growth mechanism. The initiation value $G_{IC,initiation}$ is defined from deviation of linearity and the propagation value $G_{IC,propagation}$ obtained from the average of five samples for each material at the plateau region and reported in **Table 2**. Finally, it is obvious that the MWCNTs modified CFRPs achieve higher maximum loads, which corresponds to higher critical loads during the crack propagation than the reference material.

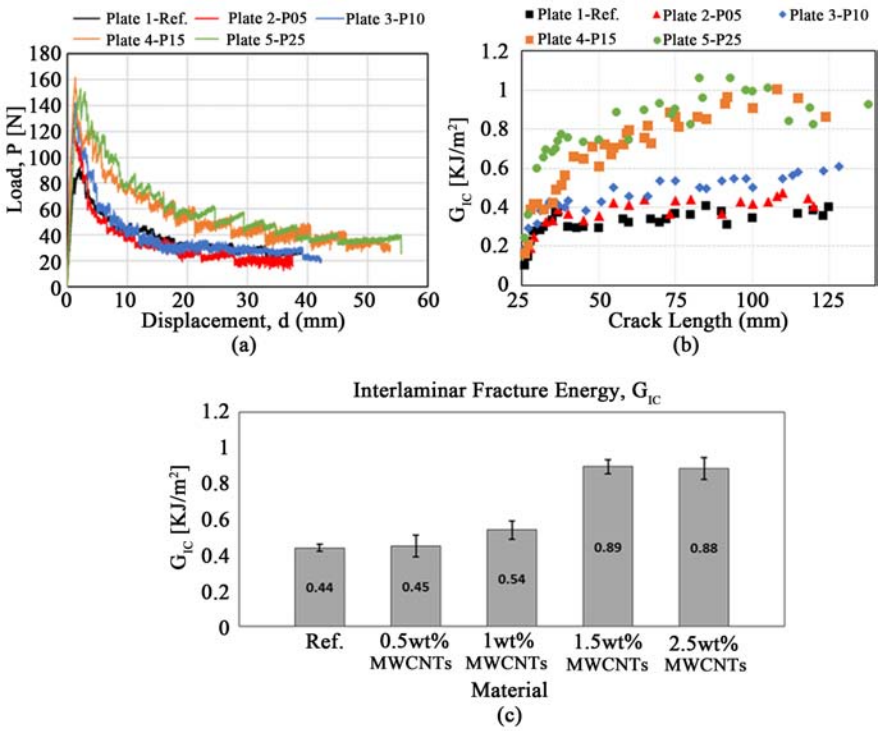

Figure 2. Mode I interlaminar fracture energy (a) load-displacement curves; (b) R curves; and (c) Strain energy release rate G_{IC} for carbon/epoxy composites with different CNTs concentrations.

Table 2. Summary of G_{IC} fracture toughness values for all tested specimens.

Laminate	MWCNTs content (wt%)	Interlaminar fracture toughness G_{IC} (KJ/m^2)			
		Initiation		Propagation	
		AVG	STDEV	AVG	STDEV
Plate 1-Ref.	0	0.16	0.03	0.44	0.02
Plate 2-P05	0.5	0.24	0.09	0.45	0.06
Plate 3-P10	1	0.23	0.04	0.54	0.05
Plate 4-P15	1.5	0.22	0.1	0.89	0.04
Plate 5-P25	2.5	0.24	0.05	0.85	0.13

Mode I fracture toughness for reference and nano-modified CFRP specimens is characterized by a crack resistance (R curves) behavior that includes an initiation value, a region of increasing toughness (resistance) as the crack extends until a steady-state value is reached, which corresponds to a self-similar crack advance. The R-curves represent the general trend of fracture toughness as a function of crack growth. As it is evident in **Figure 2(b)**, there is an initial part where crack growth resistance increases versus crack length and this part followed by a region of almost constant crack resistance value, the plateau region, (typical R curve behavior). It is clearly seen that G_{IC} values of nano-doped specimens with the addition of 1.5 wt% MWCNTs rise sharply compared to the other laminates with lower MWCNTs content. This proves the positive effect of MWCNTs fillers at highest concentration in the interlaminar fracture energy.

Mode I fracture energy for each prepared CFRP either reference or nanomodified is summarized in **Figure 2(c)**. It is clearly seen that the addition of 0.5 wt% and 1 wt% MWCNTs did not showed significant improvement in G_{IC} values, compared to reference material. On the other hand, it is evident that the addition of 1.5 wt% MWCNTs into the structure of woven fabric reinforcement caused higher improvement of G_{IC} value as it is compared against with the reference material. More precisely, the integration of 1.5 wt% MWCNTs achieved the highest increase of 103% in G_{IC}. Finally, it was concluded that further increase of MWCNTs content did not provide further enhancement of G_{IC} toughness due to agglomerates formation. Furthermore, the initiation value for all the nano-modified CFRPs remains almost the same, although higher that the reference one.

3.2. Mode II ENF Tests

Typical load-deflection curves of the ENF tests for reference and nano-doped laminates are given in **Figure 3(a)**. All specimens for each type of material showed a similar behavior. More precisely, the applied load increases linearly until the onset of the crack propagation, which is indicated by the deviation from the elastic region. The load-displacement behavior of each material is different. As a first conclusion the slope of load displacement curve of the reference

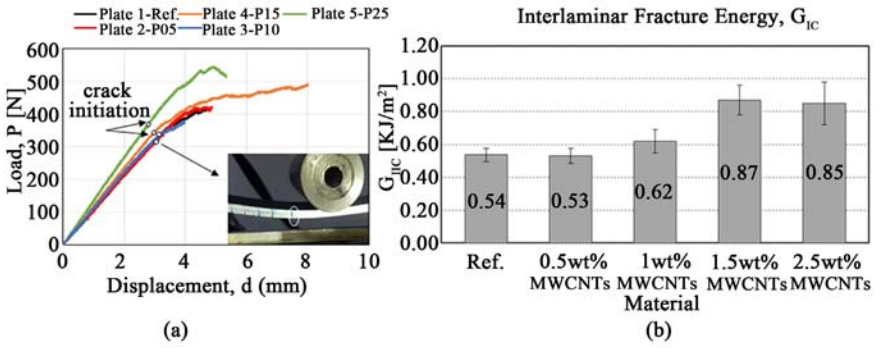

Figure 3. Mode II Interlaminar Fracture Toughness (a) load-displacement curves and (b) comparison of average G_{IIC} for carbon/epoxy composites with different CNTs concentrations.

material almost coincides with the slop of the low content MWCNTs modified composites (0.5 and 1.0 wt%). For higher MWCNTs content this slope is slightly increased, and this is more significant in the case of 2.5 wt% MWCNTs content. Furthermore, for the reference plate the applied load increases linearly until the onset of the pre-crack propagation where the load drops. On the other hand, in the case of MWCNTs modified CFRPs with higher concentrations (1.5 and 2.5 wt% MWCNTs) the linear load-displacement relationship is followed by a distinguishable deviation from linearity and much later the load drop appears. The average values and standard deviations for all manufactured CFRP plates are presented in **Figure 3(b)**. As we can see, the addition of 0.5 wt% MWCNTs did not lead to any enhancement of G_{IIC} compared to the reference material, while marginally enhancement (16%) achieved with the addition of 1 wt%. On the other hand, the introduction of higher amount of MWCNTs in to the woven fabric reinforcement caused a significant improvement in Mode II fracture toughness. More precisely, the increase in G_{IIC} achieved in the case of 1.5 wt% MWCNTs nano-modified composite is of 62% compared to reference laminate without further improvement succeeded in the case of 2.5 wt%. This is in complete agreement with the results presented earlier for G_{IC} and the explanation is again the formation of CNT agglomerates that violate structural integrity does not further promote interlaminar fracture toughness.

Table 3 summarizes the increase achieved in Mode I and Mode II interlaminar fracture toughness of the composite laminates compared against the reference material, with the incorporation of various amounts of MWCNTs into the carbon fabric reinforcement. Taking into consideration the results presented above, we can conclude that the introduction of 1.5 wt% MWCNTs into the woven fabric reinforcement significantly increase the fracture toughness of resulted CFRPs compared against the reference one. This increase is associated to additional toughening/energy dissipation mechanisms that have been incorporated into the material structure during the interlaminar crack propagation. The effect of the energy absorption mechanisms introduced by MWCNTs is mainly demonstrated at the higher amount of MWCNTs used for the nano-modification

Table 3. Summary of fracture toughness improvement compared to reference material.

Laminate	MWCNTs content (wt%)	G_{IC} increase compared to Reference	G_{IIC} increase compared to Reference
Plate 1-Ref.	0	-	-
Plate 2-P05	0.5	3%	0%
Plate 3-P10	1	23%	16%
Plate 4-P15	1.5	103%	62%
Plate 5-P25	2.5	101%	58%

of the woven fabric reinforcement. This effect is marginal in the case of lower MWCNTs content, especially under mode II remote loading.

3.3. Fractographic Analysis

The morphology and microstructure of fracture surfaces of the tested composites were also investigated by scanning electron microscopy analysis (SEM) after Mode I and Mode II tests in regions closed to the nano-modified carbon fibers. This SEM examination was used in order to confirm the additional toughening mechanisms that have been introduced by MWCNTs that were responsible for the improvement in both G_{IC} and G_{IIC}.

Figure 4 presents the failure mechanisms that were observed in the case of MWCNTs contents (0, 0.5, 1, 1.5 and 2.5 wt%). The reference CFRP composite has a very smooth fracture surface, as observed in Figure 4(a) that indicates the brittle behavior of epoxy resin. Furthermore, depicts the crack propagation along the fiber-matrix interface revealing a weak interfacial adhesion between fabric and matrix. Figure 4(b) presents the fracture surface of composite containing 0.5 wt% MWCNTs. A smooth fracture surface is still exhibited, as observed in the reference material. Additionally, a small presence of carbon nanotubes is revealed in the fiber-matrix interface. Towards this direction, in the case of 0.5 wt% MWCNTs the interlaminar fracture energy both for G_{IC} and G_{IIC} is not increased due to the absence of significant additional energy absorption mechanisms.

Figure 4(c) and Figure 4(d) present the main failure mechanisms that were observed during fracture in the cases of the increasing contents (1 and 1.5 wt% MWCNTs), respectively. By the micrographs captured at different magnifications, carbon nanotubes were distributed uniformly into the material's structure and the absence of MWCNT agglomerates was verified. Also, along the fracture surfaces it was observed that carbon nanotubes were pulled-out operating as crack-bridging elements. The red framed areas and the red arrows at these figures indicate the pull-out toughening mechanisms that were activated with the introduction of MWCNTs. This toughening mechanism indicates that the carbon nanotubes operate as crack-bridging elements and resists to crack opening and interlaminar crack propagation. In parallel, due to the presence of MWCNTs that acts as micro-pins along the crack front, in some cases these micro-pins

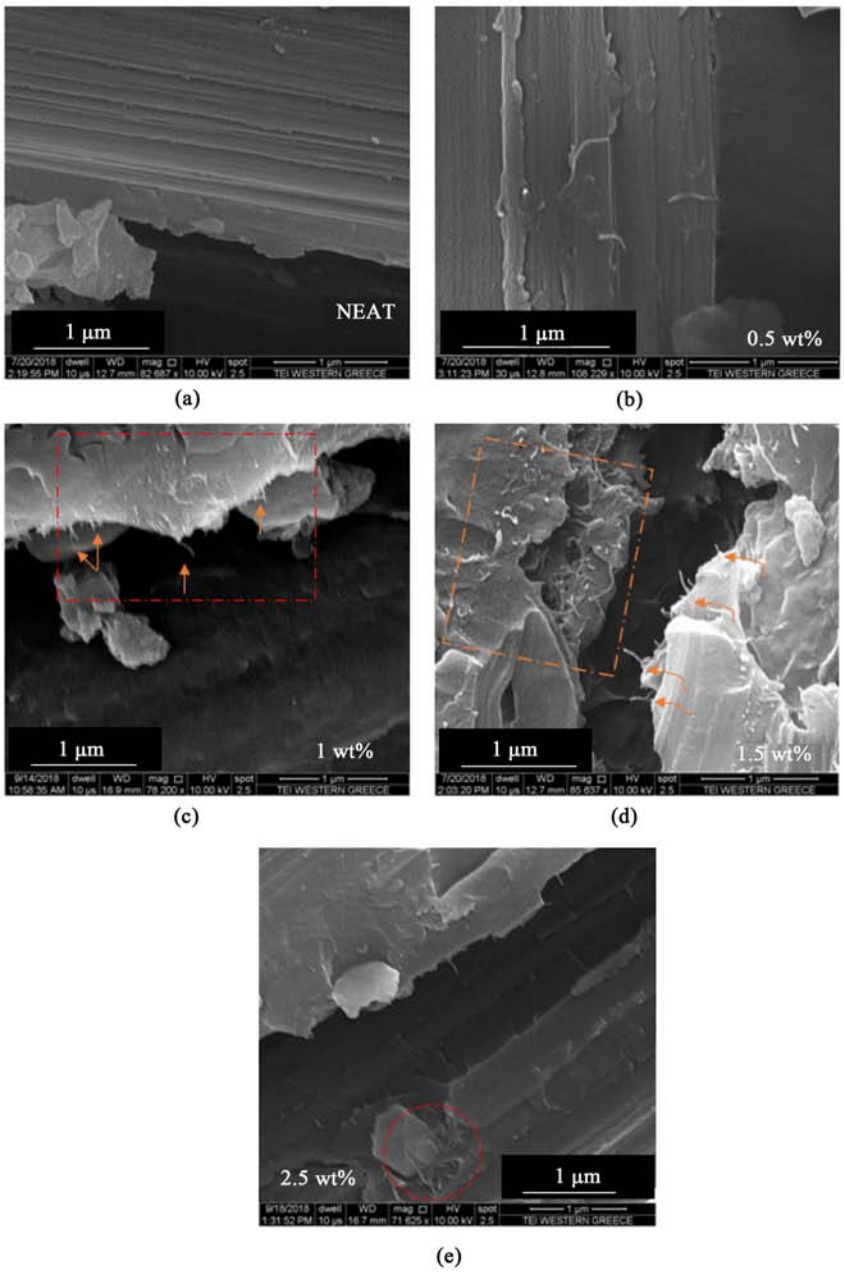

Figure 4. SEM images of fracture surface of reference material (a); nano-reinforced composites with 0.5 (b); 1 (c); 1.5 (d) and 2.5 (e) wt% MWCNTs after Mode I and Mode II tests at different magnifications.

promote crack bifurcation whenever the micro-pins cannot be removed or broken. All these additional energy absorption mechanisms contribute at macroscale, to the increase of composite interlaminar fracture energy at the CNT concentration (1.5 wt% MWCNTs). Finally, the slight degradation of fracture properties observed, in the case of nano-modified CFRP samples with the highest concentration, is associated to the presence of a small size of agglomerates, circled in Figure 4(e). This is supposed that this observation may be in whole structure.

4. Conclusion

In this work, multi-walled carbon nanotubes (MWCNTs) fillers were utilized for the development of multi-scale laminated composite for Out-of-Autoclave (OoA) manufacturing processes. Towards this direction, a nano-modified solution enriched with multi-walled carbon nanotubes was prepared while the development of nano-modified carbon fiber/epoxy laminates was produced using vacuum assisted infusion process. The objective of this study is the investigation of interlaminar fracture toughness of nano-modified CFRPs at different CNTs contents (0.5, 1, 1.5 & 2.5 wt%). The fracture toughness and the fractographic analysis of these composites were performed to assess the contribution of carbon nanotubes to the interlaminar fracture toughness of the resulted composites. The fracture toughness of nano-modified laminates showed no significant difference with respect to the reference composites in the case of low wt% MWCNTs content. Higher amount of MWCNTs at the level of 1.5 wt% increase significantly both mode I and mode II interlaminar fracture toughness of the composite laminate compared to the reference material and an increase of 103% and 62% respectively was achieved. Higher amount of MWCNTs lead to massive agglomerations and violate the positive effect of the nano-phase in energy absorption. The present MWCNTs activate at microscale energy absorption mechanisms such as bridging, and crack bifurcation thus resulting in an increase of the interlaminar fracture toughness at macroscale both under mode I and mode II remote loading.

Acknowledgements

The authors gratefully acknowledge the support of Dr. Kalarakis Alexandros for his assistance to SEM characterization of the fracture surfaces of the composites.

Conflicts of Interest

The authors declare no conflicts of interest regarding the publication of this paper.

References

[1] Mouritz, A.P. (2007) Review of Z-Pinned Composite Laminates. *Composites Part A*: *Applied Science and Manufacturing*, **38**, 2383-2397. https://doi.org/10.1016/j.compositesa.2007.08.016

[2] Cartié, D.D.R., Troulis, M. and Partridge, I.K. (2006) Delamination of Z-Pinned Carbon Fibre Reinforced Laminates. *Composites Science and Technology*, **66**, 855-861. https://doi.org/10.1016/j.compscitech.2004.12.018

[3] M'membe, B., Gannon, S., Yasaee, M., Hallett, S.R. and Partridge, I.K. (2016) Mode II Delamination Resistance of Composites Reinforced with Inclined Z-Pins. *Materials & Design*, **94**, 565-572. https://doi.org/10.1016/j.matdes.2016.01.051

[4] Dransfield, K., Baillie, C. and Mai, Y.W. (1994) Improving the Delamination Resistance of CFRP by Stitching—A Review. *Composites Science and Technology*, **50**, 305-317. https://doi.org/10.1016/0266-3538(94)90019-1

[5] Göktaş, D., Kennon, W.R. and Potluri, P. (2017) Improvement of Mode I Interlaminar Fracture Toughness of Stitched Glass/Epoxy Composites. *Applied Composite Materials*, **24**, 351-375. https://doi.org/10.1007/s10443-016-9560-x

[6] Fishpool, D.T., Rezai, A., Baker, D., Ogin, S.L. and Smith, P.A. (2013) Interlaminar Toughness Characterisation of 3D Woven Carbon Fibre Composites. *Plastics Rubber and Composites*, **42**, 108-114. https://doi.org/10.1179/1743289812Y.0000000036

[7] Unnikrishnan, K.P. and Thachil, E.T. (2006) Toughening of Epoxy Resins. *Designed Monomers & Polymers*, **9**, 129-152. https://doi.org/10.1163/156855506776382664

[8] Gorbatikh, L., Lomov, S.V. and Verpoest, I. (2011) Nano-Engineered Composites: A Multiscale Approach for Adding Toughness to Fibre Reinforced Composites. *Procedia Engineering*, **10**, 3252-3258. https://doi.org/10.1016/j.proeng.2011.04.537

[9] Borowski, E., Soliman, E., Kandil, U.F. and Taha, M.R. (2015) Interlaminar Fracture Toughness of CFRP Laminates Incorporating Multi-Walled Carbon Nanotubes. *Polymers* (*Basel*), **7**, 1020-1045. https://doi.org/10.3390/polym7061020

[10] Godara, A., Mezzo, L., Luizi, F., Warrier, A., Lomov, S.V. and van Vuure, A.W. (2009) Influence of Carbon Nanotube Reinforcement on the Processing and the Mechanical Behaviour of Carbon Fiber/Epoxy Composites. *Carbon NY*, **47**, 2914-2923. https://doi.org/10.1016/j.carbon.2009.06.039

[11] Coleman, J.N., Khan, U., Blau, W.J. and Gun'ko, Y.K. (2006) Small But Strong: A Review of the Mechanical Properties of Carbon Nanotube-Polymer Composites. *Carbon NY*, **44**, 1624-1652. https://doi.org/10.1016/j.carbon.2006.02.038

[12] Karapappas, P., Vavouliotis, A., Tsotra, P., Kostopoulos, V. and Paipetis, A. (2009) Enhanced Fracture Properties of Carbon Reinforced Composites by the Addition of Multi-Wall Carbon Nanotubes. *Journal of Composite Materials*, **43**, 977-985. https://doi.org/10.1177/0021998308097735

[13] Thostenson, E.T., Ren, Z. and Chou, T.W. (2001) Advances in the Science and Technology of Carbon Nanotubes and Their Composites: A Review. *Composites Science and Technology*, **6**, 1899-1912. https://doi.org/10.1016/S0266-3538(01)00094-X

[14] Kostopoulos, V., Baltopoulos, A., Karapappas, P., Vavouliotis, A. and Paipetis, A. (2010) Impact and After-Impact Properties of Carbon Fibre Reinforced Composites Enhanced with Multi-Wall Carbon Nanotubes. *Composites Science and Technology*, **70**, 553-563. https://doi.org/10.1016/j.compscitech.2009.11.023

[15] Kostopoulos, V., Karapappas, P., Loutas, T., Vavouliotis, A., Paipetis, A. and Tsotra, P. (2011) Interlaminar Fracture Toughness of Carbon Fibre-Reinforced Polymer Laminates with Nano- and Micro-Fillers. *Strain*, **47**, 269-282. https://doi.org/10.1111/j.1475-1305.2008.00612.x

[16] Gojny, F.H., Wichmann, M.H.G., Köpke, U., Fiedler, B. and Schulte, K. (2004) Carbon Nanotube-Reinforced Epoxy-Composites: Enhanced Stiffness and Fracture Toughness at Low Nanotube Content. *Composites Science and Technology*, **64**, 2363-2371. https://doi.org/10.1016/j.compscitech.2004.04.002

[17] Davis, D.C. and Whelan, B.D. (2011) An Experimental Study of Interlaminar Shear Fracture Toughness of a Nanotube Reinforced Composite. *Composites Part B: Engineering*, **42**, 105-116. https://doi.org/10.1016/j.compositesb.2010.06.001

[18] Zhou, Y., Pervin, F., Lewis, L. and Jeelani, S. (2008) Fabrication and Characterization of Carbon/Epoxy Composites Mixed with Multi-Walled Carbon Nanotubes. *Materials Science and Engineering: A*, **475**, 157-165. https://doi.org/10.1016/j.msea.2007.04.043

[19] Fan, Z., Santare, M.H. and Advani, S.G. (2008) Interlaminar Shear Strength of Glass Fiber Reinforced Epoxy Composites Enhanced with Multi-Walled Carbon Nanotubes. *Composites Part A*: *Applied Science and Manufacturing*, **39**, 540-554. https://doi.org/10.1016/j.compositesa.2007.11.013

[20] Qiu, J., Zhang, C., Wang, B. and Liang, R. (2007) Carbon Nanotube Integrated Multifunctional Multiscale Composites. *Nanotechnology*, **18**, Article ID: 275708. https://doi.org/10.1088/0957-4484/18/27/275708

[21] Tugrul, S.A., Tanoglu, M. and Schulte, K. (2008) Mode I and Mode II Fracture Toughness of E-Glass Non-Crimp Fabric/Carbon Nanotube (CNT) Modified Polymer Based Composites. *Engineering Fracture Mechanics*, **75**, 5151-5162. https://doi.org/10.1016/j.engfracmech.2008.08.003

[22] Sadeghian, R., Gangireddy, S., Minaie, B. and Hsiao, K.T. (2006) Manufacturing Carbon Nanofibers Toughened Polyester/Glass Fiber Composites Using Vacuum Assisted Resin Transfer Molding for Enhancing the Mode-I Delamination Resistance. *Composites Part A*: *Applied Science and Manufacturing*, **37**, 1787-1795. https://doi.org/10.1016/j.compositesa.2005.09.010

[23] Kim, K.J., Yu, W.R., Youk, J.H. and Lee, J. (2012) Factors Governing the Growth Mode of Carbon Nanotubes on Carbon-Based Substrates. *Physical Chemistry Chemical Physics*, **14**, 140-141. https://doi.org/10.1039/c2cp42566a

[24] He, X., Zhang, F., Wang, R. and Liu, W. (2007) Preparation of a Carbon Nanotube/Carbon Fiber Multi-Scale Reinforcement by Grafting Multi-Walled Carbon Nanotubes onto the Fibers. *Carbon NY*, **45**, 2559-2563. https://doi.org/10.1016/j.carbon.2007.08.018

[25] Karapappas, P., Tsantzalis, S., *et al*. (2008) Multi-Wall Carbon Nanotubes Chemically Grafted and Physically Adsorpted on Reinforcing Carbon Fibres. *Advanced Composites Letters*, **17**, 103-107. https://doi.org/10.1177/096369350801700304

[26] An, Q., Rider, A.N. and Thostenson, E.T. (2012) Electrophoretic Deposition of Carbon Nanotubes onto Carbon-Fiber Fabric for Production of Carbon/Epoxy Composites with Improved Mechanical Properties. *Carbon NY*, **50**, 4130-4143. https://doi.org/10.1016/j.carbon.2012.04.061

[27] De Greef, N., Zhang, L., Magrez, A., Forró, L., Locquet, J.P. and Verpoest, I. (2015) Direct Growth of Carbon Nanotubes on Carbon Fibers: Effect of the CVD Parameters on the Degradation of Mechanical Properties of Carbon Fibers. *Diamond and Related Materials*, **1**, 39-48. https://doi.org/10.1016/j.diamond.2014.11.002

[28] Zhang, J., Li, W., Soga, T., Jimbo, T. and Tanji, T. (2012) Synthesis of High-Density Vertically Aligned Carbon Nanotubes Using Ultrasonic Nebulizer. *Material Science and Applications*, **3**, 213-217. https://doi.org/10.4236/msa.2012.34031

[29] Zhang, H., Liu, Y., Kuwata, M., Bilotti, E. and Peijs, T. (2015) Improved Fracture Toughness and Integrated Damage Sensing Capability by Spray Coated CNTs on Carbon Fibre Prepreg. *Composites Part A*: *Applied Science and Manufacturing*, **70**, 102-110. https://doi.org/10.1016/j.compositesa.2014.11.029

[30] Resoltech Resin Resolcoat 1400 Data Sheet. https://www.resoltech.com/en/products/epoxy/1400-detail.html

[31] Pyrofil Carbon Fiber Datasheet. http://mccfc.com/pan-fiber

[32] Nanocyl Sizing Agent Data Sheet. http://www.nanocyl.com/product

[33] ASTM D 5528-01, ASTM Int. Standard Test Method for Mode I Interlaminar Fracture Toughness of Unidirectional Fiber-Reinforced Polymer Matrix Composites. Standard No. ASTM D5528-01.

[34] ASTM D 7905/D7905M-14, ASTM Int. Standard Test Method for Determination of the Mode II Interlaminar Fracture Toughness of Unidirectional Fiber-Reinforced Polymer Matrix Composites.

Scientific Research Publishing

World Journal of Mechanics, 2019, 9, 163-176
http://www.scirp.org/journal/wjm
ISSN Online: 2160-0503
ISSN Print: 2160-049X

Offside Detection System Using an Infrared Camera Tracking System

Esteban Lopez, Peter E. Jenkins*

Mechanical Engineering Department, University of Colorado, Denver, USA
Email: *peter.jenkins@ucdenver.edu

How to cite this paper: Lopez, E. and Jenkins, P.E. (2019) Offside Detection System Using an Infrared Camera Tracking System. *World Journal of Mechanics*, **9**, 163-176.
https://doi.org/10.4236/wjm.2019.96011

Received: May 29, 2019
Accepted: June 25, 2019
Published: June 28, 2019

Abstract

This paper describes an experimental offside detection system that will be capable of detecting offside passes during a game of soccer. Soccer is the world's most popular and most televised sport. In recent years, FIFA has implemented goal line technology in order to end controversial goals/missed goals during high profile competitive matches. The most contentious aspect of the sport is the offside rule and its many controversial calls or lack of calls. Sometimes the linesmen cannot see the passage of playing fast enough to make a correct decision. Being similar to goal line technology, people have requested offside technology to help the linesmen and to reduce the number of incorrect offside calls in a game. This paper describes a working offside detection system that can accurately detect offside passes. Positional data was exported from a VICON infrared motion tracking camera system and a MATLAB script was written so that it can analyze the positions of the players and the ball and determine if a pass was offside.

Keywords

Soccer, Motion Simulation

1. Introduction

The purpose of this project is to design and develop an experimental offside detection system that will be capable of detecting offside passes during a game of soccer. Soccer is the world's most popular and most televised sport. Every year, thousands of players from all across the world compete in some of the most competitive and prestigious leagues. In recent years, FIFA [1], soccer's governing body, has implemented goal line technology in order to end controversial goals/missed goals during high profile competitive matches. This has been a step in the right direction, however, there are still many issues in the world of soccer.

The most contentious aspect of the sport is the offside rule and its many controversial calls or lack of calls. There have been countless instances when a player is wrongfully ruled offside after scoring a game changing goal. There have also been many cases in which a player has scored a game winning goal and the player was not ruled to be offside when the play should have been stopped. Incorrect offside calls have the potential to ruin games. Sometimes the linesmen, the referees in charge of judging offside calls, cannot see the passage of playing fast enough to make a correct decision. There are many cases in which a ball is played too quickly for anyone to make the correct call. Being similar to goal line technology, people have called out for offside technology to help the linesmen and to reduce the number of incorrect offside calls in a game. That is why the objective of this project is to create a working offside detection system that can accurately detect offside passes. Positional data will be exported from the system and a MATLAB script will be written so that it can analyze the positions of the players and the ball and determine if a pass was offside.

2. Methods

1) The Offside Rule

In order to understand how this offside detection system is going to function, one must understand the offside rule first. The offside rule is defined as follows [2]: "A player is offside when he/she is nearer to the opponent's goal line than the second to last opponent when the ball is played/passed from one player to the player that is nearest to the goal line. Being level with the second to last opponent does not constitute being offside, neither does being level with both the last two opponents if they happen to be in line". When judging the condition of being "nearer", only a player's head, torso, legs, and feet are taken into consideration. The player's arms do not count. A player cannot be offside in his/her own half of the pitch regardless of where he/she is positioned in relation to the ball or members of the opposing team. In order for a player to be considered offside, he/she must be involved in active play. This can be accomplished in two ways. One is to be interfering with the play, or if the player is interfering with an opponent.

2) VICON System Specifications & Setup

A VICON motion tracking camera system [3] and software was used for the development of this system. The College of Arts & Media currently has a VICON system in the Digital Animation Center (DAC). This VICON system consists of 20 Bonita 10 infrared tracking cameras and they are placed along the edges of the room. The cameras all face the center of the room where an 18' × 14' space is designated for digital motion tracking. Each Bonita 10 camera has a maximum frame rate of 250 fps. The lens has an operating range of 13 meters and a maximum field of vision that is 70.29˚ × 70.29˚. The DAC normally uses a VICON software called BLADE for their animation and motion capture needs. Fortunately, VICON also provides a software called Tracker which tracks the

positions of rigid bodies and exports that data as a file, or in real time if needed. VICON was generous and provided a free month-long trial of their Tracker software for this project. The Bonita 10 cameras track rigid bodies via the use of reflective markers. In order to create a rigid body in the system, the reflective markers need to be grouped into unique clusters [4]. Each pattern must be unique, otherwise the cameras will confuse one cluster for another and combine or remove desired rigid bodies. Figure 1 shows some of the reflective markers used in this project.

Once the reflective markers have been put into unique clusters, the next step is to strap them onto the desired rigid bodies. In this project, the objects that need to be tracked are each player's legs, torso, and head. There are four players involved in this simulation, so a total of four heads, four torsos, and eight legs need to be tracked. Figure 2 shows an example of how the markers were strapped onto the players.

Once each player has been strapped with their designated markers, the next step is to use the Tracker software to create the rigid bodies. Once the cameras have been calibrated and set, the software will recognize each marker and each unique pattern and create a rigid body. Each rigid body can be labeled so that one can keep track of which rigid body belongs to each player. Figure 3 shows how each rigid body is represented in the software for each player and the ball.

Additionally, the ball that will be used during this project also needs to be tracked by the VICON camera system. Since the reflective markers that are used to track the players are spheres, they cannot be used to track the ball. The reflective markers would keep the ball from rolling. The solution to this problem was

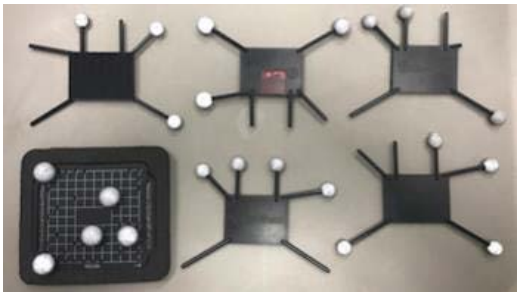

Figure 1. Reflective markers for rigid body tracking.

Figure 2. Reflective marker set up.

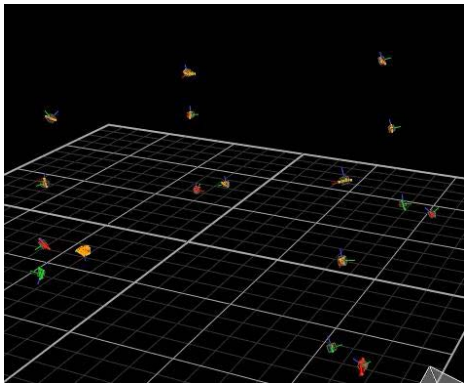

Figure 3. Rigid bodies as shown on VICON Tracker software.

to use OptiTrack reflective tape. The reflective tape was cut into small circles and placed in unique patterns across the ball so that the software could identify the ball as its own rigid body. Figure 4 shows the ball and the reflective tape used for tracking.

3) Single Pass Simulation

In this project, simulations were conducted with four players. Players 1 and 2 were part of Team A. Team A was the attacking team making the passes. Players 3 and 4 were part of Team B. Team B was the defending team setting the offside line. Figure 5 shows the position of both teams before and after the single pass was made.

It can be seen that the only object that moves is the ball. This was a way to control the offside line in order to ensure that they algorithm correctly identified the type of pass. In this situation, the ball is at rest and is passed only once. This simulation was conducted twice. Once for an onside pass and once for an offside pass. In the first pass, player 1 passes the ball to player 2. Both players are behind players 3 and 4, and therefore onside. In the second pass, player 2 is in front of players 3 and 4 and therefore in an offside position. Figure 6 shows the loop in the algorithm that was used to determine the frames in which the ball was moving and shows the first 22 frames.

The loop runs through all the position changes in the X-direction of the ball and finds any frame where the ball has traveled more than 10 millimeters. Once it has found these frames, it places them in the vector shown in Figure 6. The first frame in the vector is where the pass was made. The rest of the algorithm would then find the player's position at this frame and determine if the pass was onside or offside. This report will not go into further detail about the methods used for the single pass scenarios. This report will instead have an in depth look at the methods used for the final running simulation [5].

4) Final Running Simulation

Once the code had been created for a single pass, the next step was to modify the algorithm and run a simulation where all players are constantly changing positions, thus changing the offside line. Figure 7 shows an example of the changes in player position for the final simulation.

Figure 4. Ball and its reflective markers.

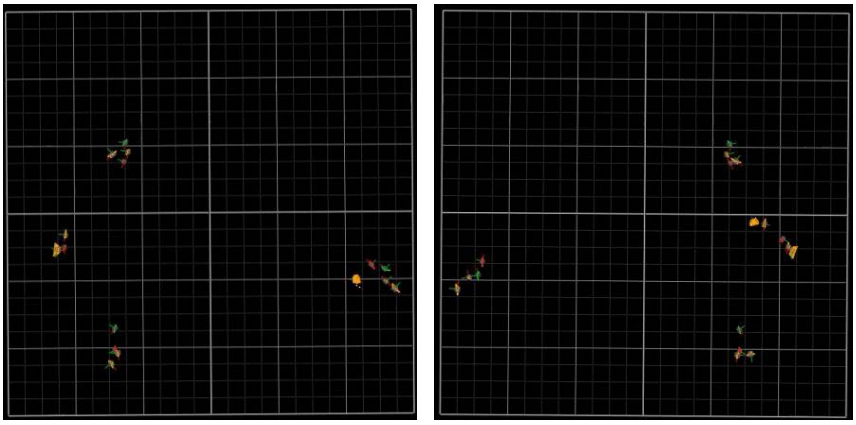

Figure 5. Static trial player positions before & after pass.

```
%% Onside Forward Pass
%%% Analyzing the Ball

%Calculate Row Deltas
D_Ball = diff(Ball);
Deltas_Ball = abs(D_Ball);

k = find(Deltas_Ball(:,4)>10);
z = Deltas_Ball(k,4);

movingFrames = [];
index = 1;
for i=1:(length(k)-1)
    delta = k(i+1)-k(i);
    if delta<2
        movingFrames(index) = k(i);
        index = index + 1;
    end
end

movingFrames = movingFrames';
%A Pass is started at movingFrames(1) at this point in the code
%Now need to compare the positions of all players at the index/frame...
%when pass was made. i.e if pass made at frame 466. Find position...
%of all players at frame 466 and compare.
```

movingFrames

123x1 double

	1	2
1	157	
2	158	
3	159	
4	160	
5	161	
6	162	
7	163	
8	164	
9	165	
10	166	
11	167	
12	168	
13	169	
14	170	
15	171	
16	172	
17	173	
18	174	
19	175	
20	176	
21	177	
22	178	

Figure 6. Loop to determine moving frames.

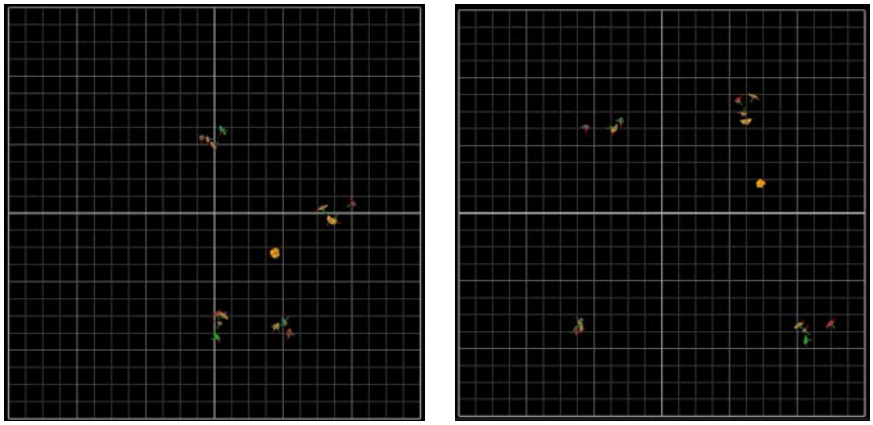

Figure 7. Running simulation player positions changing with time.

This running simulation is the final run that is to be analyzed by the algorithm. For this project, the running simulation lasted 2 minutes and 9 seconds. The code was altered so that it could read all passes sequentially. In order for the algorithm to detect passes, the positional data needed to be loaded onto MATLAB. The data for each rigid body was exported as an excel file. Figure 8 shows the way the data was formatted for all rigid bodies.

The software tracks six different types of positional data for each rigid body. Columns one through three are the rotational positions in the X, Y, and Z directions. These are measured in radians. Columns four through six are the translational positions in the X, Y, and Z directions. These are measured in millimeters. This project will only focus on columns four through six for each rigid body since the translational data is what will be analyzed. In this simulation, the ball was passed under three different conditions. The first type of pass that was observed was when the ball was at rest and was then kicked. In order to determine when the ball was kicked, the code looks at the changes in the X-direction. If the changes in the X-direction went from less than 10 mm per frame to greater than 10 mm per frame, then the ball was considered to be in motion, and thus passed at that specific frame. Figure 9 shows the changes in the X-direction for the ball at frame 2944.

The majority of the passes happened under these conditions. Figure 10 shows how the code was written to capture the frames where these pass conditions were met.

The second type of pass that was observed was when the ball was passed vertically. In this scenario, the code needed to read the changes in the Y-direction for the ball. The same conditions were applied as in the first type of pass. If the changes in the Y-direction went from less than 10 mm per frame to greater than 10mm per frame, then the ball was considered to be in motion, thus passed at that specific frame. Figure 11 shows the changes in the Y-direction for the ball.

Only one pass fell under this criterion and that was at frame 561. Figure 12 shows how the code was written to determine the frame where this pass condition was met.

		Global Angle Player_3_Head: Player_3_Head					
Frame	Sub Frame	RX	RY	RZ	TX	TY	TZ
		rad	rad	rad	mm	mm	mm
1	0	-0.420662	0.539482	4.0564	697.985	-1718.96	1613.23
2	0	-0.397319	0.521966	4.04231	701.481	-1716.14	1613.43
3	0	-0.407936	0.531558	4.04906	705.444	-1714.86	1613.23
4	0	-0.39644	0.514076	4.043	709.124	-1711.97	1613.28
5	0	-0.406556	0.516764	4.04654	712.853	-1710.84	1612.92

Figure 8. Exported positional data for player 3 head first five frames.

	1	2	3	4	5	6
2932	0.0012	0.0018	0.0025	0.0610	0.0320	0.2031
2933	5.5000e-04	0.0024	5.8300e-04	0.1090	0.1640	0.0281
2934	0.0044	1.0000e-05	0.0019	0.0280	0.2130	0.1217
2935	0.0024	9.6000e-04	0.0045	0.1870	0.2850	0.2043
2936	0.0011	4.0000e-05	7.7900e-04	0.0070	0.0010	0.0414
2937	0.0011	0.0018	0.0016	0.0960	0.2620	0.0774
2938	0.0012	0.0030	0.0036	0.0860	0.2530	0.0159
2939	0.0021	0.0055	0.0028	0.0060	0.3590	0.3641
2940	0.0018	0.0020	0.0088	0.1220	0.6420	0.0041
2941	0.0016	0.0023	0.0024	0.1680	0.3130	0.0936
2942	2.5000e-04	0.0055	2.1100e-04	0.0920	0.3540	0.2038
2943	1.0000e-04	0.0099	0.0145	0.2730	0.9080	0.0635
2944	0.0318	0.0365	0.0288	11.6370	6.0090	3.6835
2945	0.0730	0.1185	0.0129	24.9890	8.1310	1.8572
2946	0.0723	0.0985	0.0070	24.2270	9.2310	1.8648
2947	0.0725	0.1002	0.0233	24.8710	9.9680	0.1990
2948	0.0852	0.0507	0.0213	24.5110	10.1580	1.0405
2949	0.0759	0.0673	0.0022	24.7050	11.0640	0.6678
2950	0.0691	0.0654	0.0026	25.3650	11.5280	1.0138
2951	0.0937	0.0511	0.0293	24.6610	9.6710	1.8980
2952	0.0784	0.0429	0.0103	24.7840	11.1140	2.6512
2953	0.0836	0.0431	0.0161	24.6250	10.7820	3.3800

Figure 9. Column 4 shows ball changes in X-direction at frame 2944 for pass Type 1.

```
%% Passes
%%% Analyzing the Ball

%Frame rate
t = 129; %seconds (run time of simulation)
fps = Frames/t;
spf = t/Frames; %seconds per frame

%Calculate Row Deltas
D_Ball = diff(Ball);
Deltas_Ball = abs(D_Ball);
%k = find(Deltas_Ball(:,4)>10);

%%%%3 scenarios where passes are made%%%
%%%Scenario 1 - Ball is at rest and then it is passed%%

Passes1 = [];
index = 1;
for i=1:(length(Deltas_Ball)-1)
    if (Deltas_Ball(i,4)<10 && Deltas_Ball(i+1,4)>10 && Deltas_Ball(i+2,4)>10 && Deltas_Ball(i+3,4)>10 && Deltas_Ball(i+4,4)>10 && Deltas_Ball(i+5,4)>10)
        Passes1(index) = i+1;
        index = index + 1;
    end
end
Passes1 = Passes1';
```

Figure 10. Pass type 1 code for determining relevant frames.

	1	2	3	4	5	6
550	0.0042	0.0091	0.0024	1.0030	0.0200	0.0260
551	0.0174	4.9100e-04	3.4000e-04	0.4040	0.3200	0.0870
552	2.2000e-04	7.7800e-04	0.0080	0.9820	0.4000	0.2220
553	0.0060	0.0032	3.3000e-04	1	0.3000	0.1190
554	0.0125	0.0115	0.0161	1.7350	0.2700	0.1800
555	0.0024	0.0027	0.0056	0.7820	0.9800	0.0740
556	0.0061	0.0082	0.0016	1.2710	0.2200	0.0650
557	0.0103	0.0014	0.0073	0.2160	0.4200	0.0390
558	0.0242	0.0068	2.8000e-04	0.0230	0.0500	0.5350
559	0.0048	0.0023	0.0012	0.9080	0.4500	0.0250
560	0.0062	0.0026	0.0018	0.5910	0.7900	0.2580
561	0.0541	0.0466	0.0026	2.1030	13.9800	0.5970
562	0.0285	0.0544	0.0041	5.4150	28.8100	0.0150
563	0.0423	0.0862	0.0192	5.2470	28.4900	1.4840
564	0.0514	0.0852	0.0128	4.9480	28.4100	0.2110
565	0.0389	0.0859	0.0124	5.0970	28.4600	0.4200
566	0.0284	0.0841	0.0092	5.4350	28.9700	1.3770
567	0.0561	0.1063	0.0094	5.0590	27.9300	1.9270
568	0.0776	0.1027	0.0101	3.4800	28.6500	0.1220
569	0.0279	0.1110	0.0296	5.2140	28.7300	1.3040

Figure 11. Column 5 shows ball changes in Y-direction at frame 561 for pass type 2.

```
%%%Scenario 2 - Ball is passed vertically so need to analyze Delta y
%%%instead of Delta x%%%

Passes2 = [];
index2 = 1;
for j = 1:(length(Deltas_Ball)-1)
    if (Deltas_Ball(j,5)< 1 && Deltas_Ball(j+1,5)>10 && Deltas_Ball(j,2)<.003)
        Passes2(index2) = j+1;
        index2 = index2 + 1;
    end
end

Passes2 = Passes2';
```

Figure 12. Pass type 2 code for determining relevant frame.

The final type of pass that was observed was when the ball had already been passed and was passed again by the receiving player while the ball was still in motion. In this scenario, the ball was never at rest between passes and thus needed to be analyzed in a different way. For this scenario, the velocities of the ball at each frame were determined. If the changes in the X-direction were greater than 10 mm per frame, but there was a sign change in the velocities, then the frames where the sign changes occurred were considered a pass. **Figure 13** shows the changes in the X-direction for the ball at frame 2304.

There is a sign change in the velocities at frame 2304 (**Figure 14**). This means that a pass was made at this frame. **Figure 15** shows how the code was written to calculate the velocities at each frame and how the sign changes were found.

Finally, once pass frames had been isolated, various loops were created in the algorithm that would compare the positions of each player's legs, torso, and head at those frames. A final loop was created to compare those positions between the attacking players and the defending players. **Figure 16** shows how the player's positions at all relevant frames were found.

The final section in the algorithm then determined if the pass was onside or offside. **Figure 17** shows the final loops in the code that determined offside passes.

3. Results

The results for the single pass simulations can be seen on **Table 1**.

The results determined from the algorithm match the results that were obtained by visually confirming the pass from the simulation videos that were recorded from the software.

The running simulation is more complex than the single pass simulations. In order to determine the number of passes and their status, the frames where the passes were made needed to be determined. **Table 2** shows the number of passes and their corresponding frames.

There were 45 passes in total throughout this simulation. However due to glitches in the system as well as gaps in the data due to camera limitations, only 43 out of the 45 passes were recognized by the cameras. This is further explained in the Discussion section of this report. The missing passes did not affect the

	1	2	3	4	5	6
2296	0.0202	0.0679	0.0040	12.0100	2.9770	7.1770
2297	0.0229	0.2066	0.0189	13.8700	4.2330	11.6390
2298	0.0351	0.2045	0.0156	15.9900	3.1270	11.4400
2299	0.0193	0.0993	0.0122	15.9300	4.7620	7.0960
2300	0.0439	0.0904	0.0094	16.1900	3.9970	6.4670
2301	0.6299	0.0700	0.7086	55.4400	17.8960	32.0290
2302	0.0792	0.1349	0.0197	15.0100	1.5640	0.7700
2303	0.0715	0.1571	0.0723	12.4900	3.1340	0.2990
2304	0.0167	0.0334	0.0070	19.1200	1.8270	2.2880
2305	0.0718	0.1268	0.0452	36.1600	6.0230	2.5560
2306	0.0323	0.1060	0.1390	33.1600	2.4410	2.0390
2307	0.0415	0.1446	0.1451	31.5400	2.8470	0.5460
2308	0.0592	0.1138	0.1212	32.4200	0.6880	0.8540
2309	0.0691	0.1274	0.1290	31.6600	1.2480	1.7510
2310	0.1152	0.1336	0.1642	29.8500	2.6560	0.9710
2311	0.0888	0.1467	0.1136	31.2200	0.3010	3.5010
2312	0.0581	0.1643	0.0935	31.0600	0.6410	4.5100
2313	0.1358	0.1736	0.1073	29.2000	0.3300	1.0740

Figure 13. Columns 4 shows ball changes in X-direction at frame 2304 for pass type 3.

	1
2296	-1.2072e+03
2297	-1.3942e+03
2298	-1.6073e+03
2299	-1.6013e+03
2300	-1.6274e+03
2301	-5.5728e+03
2302	-1.5088e+03
2303	-1.2555e+03
2304	1.9219e+03
2305	3.6348e+03
2306	3.3332e+03
2307	3.1704e+03
2308	3.2588e+03
2309	3.1824e+03
2310	3.0005e+03
2311	3.1382e+03
2312	3.1221e+03
2313	2.9352e+03

Figure 14. Shows the calculated velocities for the frames around frame 2304.

```
%%%Scenario 3 - Ball is passed immedietly after receiving ball%%
%%%Ball never stops rolling and is passed from on direction to the next%%%
%%%Need to check velocities for sign changes%%%

v1 = D_Ball(:,4)/spf; %mm/s

Passes3 = [];
index3 = 1;
for k = 1:(length(v1)-3)
    if (v1(k)<0 && v1(k+1)<0 && v1(k+2)>1340 && v1(k+3)>0) %&& v1(k+4)>0 && v1(k+5)>0 && v1(k+6)>0 && v1(k+7)>0)
        Passes3(index3) = k+2;
        index3 = index3 + 1;
    end
end

Passes3 = Passes3';
```

Figure 15. Pass type 3 code for determining relevant frames.

Table 1. Results for the single pass simulations.

Onside Static Pass		Offside Static Pass	
Frame	Status	Frame	Status
466	Onside	157	Offside

```
%% Analyzing Players Positions at Pass

P1_H_Value = [];P2_H_Value = [];P3_H_Value = [];P4_H_Value = [];
P1_LL_Value = [];P2_LL_Value = [];P3_LL_Value = [];P4_LL_Value = [];
P1_RL_Value = [];P2_RL_Value = [];P3_RL_Value = [];P4_RL_Value = [];
P1_T_Value = [];P2_T_Value = [];P3_T_Value = [];P4_T_Value = [];
ind = 1;
for i=1:length(Passes)
    %Player 1
    P1_H_Value(ind) = P1_Head(Passes(i),4);
    P1_LL_Value(ind) = P1_LL(Passes(i),4);
    P1_RL_Value(ind) = P1_RL(Passes(i),4);
    P1_T_Value(ind) = P1_T(Passes(i),4);

    % Player 2
    P2_H_Value(ind) = P2_Head(Passes(i),4);
    P2_LL_Value(ind) = P2_LL(Passes(i),4);
    P2_RL_Value(ind) = P2_RL(Passes(i),4);
    P2_T_Value(ind) = P2_T(Passes(i),4);

    % Player 3
    P3_H_Value(ind) = P3_Head(Passes(i),4);
    P3_LL_Value(ind) = P3_LL(Passes(i),4);
    P3_RL_Value(ind) = P3_RL(Passes(i),4);
    P3_T_Value(ind) = P3_T(Passes(i),4);

    % Player 4
    P4_H_Value(ind) = P4_Head(Passes(i),4);
    P4_LL_Value(ind) = P4_LL(Passes(i),4);
    P4_RL_Value(ind) = P4_RL(Passes(i),4);
    P4_T_Value(ind) = P4_T(Passes(i),4);

    ind = ind+1;
end
P1_H_Value = P1_H_Value';P2_H_Value = P2_H_Value';P3_H_Value = P3_H_Value';P4_H_Value = P4_H_Value';
P1_LL_Value = P1_LL_Value';P2_LL_Value = P2_LL_Value';P3_LL_Value = P3_LL_Value';P4_LL_Value = P4_LL_Value';
P1_RL_Value = P1_RL_Value';P2_RL_Value = P2_RL_Value';P3_RL_Value = P3_RL_Value';P4_RL_Value = P4_RL_Value';
P1_T_Value = P1_T_Value';P2_T_Value = P2_T_Value';P3_T_Value = P3_T_Value';P4_T_Value = P4_T_Value';
```

Figure 16. Code for determining player positions at relevant frames.

```
%% Determining Onside/Offside Pass

A_Attacking = [A1 A2];
A_Offside = [A3 A4];
Offside_Line = [];
ind2 = 1;
for i=1:length(A_Offside)
    Offside_Line(ind2) = max(A_Offside(i,:));
    ind2 = ind2 + 1;
end

Offside_Line = Offside_Line';


V_final = [];
ind3 = 1;
for i=1:length(Passes)
    V_final(ind3) = v1(Passes(i));
    ind3 = ind3 + 1;
end
V_final = V_final';

Pass_Decision = {};
ind4 = 1;
for i=1:length(Offside_Line)
    if (max(A_Attacking(i,:)) > Offside_Line(i) && V_final(i) > 0)
        Pass_Decision{ind4} = {'OFFSIDE'};
        ind4 = ind4 + 1;
    elseif (max(A_Attacking(i,:)) < Offside_Line(i) || V_final(i) < 0)
        Pass_Decision{ind4} = {'Onside'};
        ind4 = ind4 + 1;
    end
end

Pass_Decision = Pass_Decision';
Pass_Numbers = [1:length(Passes)]';
T = table(Pass_Numbers, Pass_Decision);
```

Figure 17. Final loops for determining offside passes.

Table 2. Number of passes & corresponding frames their corresponding frames.

Pass	Status	Pass	Status	Pass	Status	Pass	Status	Pass	Status
1	108	11	2944	21	5687	31	8771	41	12,037
2	329	12	3206	22	5957	32	9591	42	12,320
3	561	13	3446	23	6178	33	10,039	43	12,420
4	903	14	3723	24	6398	34	10,347		
5	1178	15	4016	25	6612	35	10,574		
6	1354	16	4342	26	7105	36	10,854		
7	1631	17	4621	27	7569	37	11,120		
8	1869	18	4907	28	7836	38	11,362		
9	2144	19	5218	29	8237	39	11,612		
10	2304	20	5485	30	8468	40	11,781		

results of this project. Once the number of passes and their corresponding frames had been identified, the algorithm was able to determine whether each pass was onside or offside. Table 3 shows the final results of the running simulation for each pass. Table 4 shows the results from the visual confirmation of each pass and is favorably compared to the simulation results given in Table 4.

4. Conclusion

In conclusion, the offside detection system prototype has successfully identified onside and offside passes. Table 3 and Table 4 in the results section are identical. This means that the algorithm accurately determined the status of all 43 passes in the simulation. The success of the prototype is a major step towards the advancement of technology in soccer.

5. Discussion

Even though the prototype was a success, there were some limitations to the design. The biggest limitation to the design was the fact that the Tracker software was not meant to track a large number of rigid bodies at once. Since each rigid body had to be comprised of a unique pattern of reflective markers, it became difficult to have enough different patterns for each rigid body as the number of rigid bodies increased. Additionally, the software would sometimes confuse one rigid body for another if two players got to close to one another. If one player ran past another, there were instances where the markers on one player's leg were too close to another player's leg, thus creating one rigid body that the software could not recognize. As a result, there are gaps in the data that was exported from the software. Fortunately, these gaps did not occur at the instances where the passes were made. However, moving forward, this could be an issue if the gaps were to occur during important sections of the simulations.

Gaps in the data did not only occur when multiple rigid bodies got too close to one another. They also occurred whenever the ball was in motion. Since the

Table 3. Pass results from algorithm.

1 Pass_Numbers	2 Pass_Decision
1	Onside
2	Onside
3	Onside
4	Onside
5	Offside
6	Onside
7	Onside
8	Onside
9	Onside
10	Offside
11	Onside
12	Onside
13	Onside
14	Offside
15	Onside
16	Onside
17	Onside
18	Offside
19	Onside
20	Offside
21	Onside
22	Onside
23	Offside
24	Onside
25	Offside
26	Onside
27	Onside
28	Onside
29	Offside
30	Onside
31	Offside
32	Onside
33	Offside
34	Onside
35	Offside
36	Onside

Continued

37	Offside
38	Onside
39	Offside
40	Onside
41	Onside
42	Onside
43	Onside

Table 4. Pass results from visual confirmation of simulation recordings.

Pass	Status	Pass	Status	Pass	Status	Pass	Status	Pass	Status
1	Onside	11	Onside	21	Onside	31	OFFSIDE	41	Onside
2	Onside	12	Onside	22	Onside	32	Onside	42	Onside
3	Onside	13	Onside	23	OFFSIDE	33	OFFSIDE	43	Onside
4	Onside	14	OFFSIDE	24	Onside	34	Onside		
5	OFFSIDE	15	Onside	25	OFFSIDE	35	OFFSIDE		
6	Onside	16	Onside	26	Onside	36	Onside		
7	Onside	17	Onside	27	Onside	37	OFFSIDE		
8	Onside	18	OFFSIDE	28	Onside	38	Onside		
9	Onside	19	Onside	29	OFFSIDE	39	OFFSIDE		
10	OFFSIDE	20	OFFSIDE	30	Onside	40	Onside		

software needs to see all reflective tape marks on the ball in order to establish it as a rigid body, the bottom portion of the ball did not have any reflective tape on it. This resulted in gaps in the data whenever the ball rolled since the bottom portion of the ball would end up on top while in motion. When this happened, the cameras would momentarily lose track of the ball for a few frames. The cameras would detect the ball once it had completed a rotation and all pieces of tape were visible yet again. These gaps in the data affected two of the passes during the simulation. Frames 9175 and 12,202 saw two short and quick passes between players 1 and 2. Since there were gaps in the data, the software did not track these passes. Fortunately, both of these passes were onside and happened at a short distance where they did not affect the results of the simulation. All offside passes were accurately tracked and were not affected by the gaps in the data. Additionally, there were some movement restrictions throughout this project. The VICON system was located inside a computer lab/classroom, therefore all passes needed to remain on the ground. The ball needed to be passed at a reasonable speed so that no equipment or students would get injured.

Moving forward there are many improvements that could be made to this experimental offside detection system. The main improvement that can be made is to improve the camera system. The VICON system works great and the infrared

tracking is accurate. However, in a real game setting this system will be impossible to use. The infrared tracking will simply not work in an outdoor environment. In order for the cameras to detect the reflective markers, there needs to be zero sunlight in the room and all other reflective surfaces need to be covered up. Additionally, in a real game setting it is not practical to have spherical trackers on the player's bodies. One solution is to utilize reflective tape on the players so that they can move as they normally would. However, this would only be practical in an indoor setting. The best way to move forward is to adopt a camera system that uses artificial intelligence and machine learning to detect color and track objects based on color. There have been numerous research studies done within the last 10 years and the technology is there. In a real game setting these cameras can be used outdoors and would be able to track the colors of each team's jerseys. The VICON system does however work accurately and effectively in terms of the scope of this project. This project is the foundation for what is meant to be a radical change in the world of soccer. Offside technology is years away from being perfected, however this project has demonstrated that it can be done accurately and effectively given the proper resources. The purpose of this project has been completed and the main objective has been met. The VICON infrared camera system can accurately detect offside passes. This technology can be used to aid the referees and officials to fairly influence the outcome of soccer games.

Acknowledgements

1) The authors would like to thank the University of Colorado Denver Digital Animation Center.

2) The support of VICON was appreciated.

Conflicts of Interest

The authors declare no conflicts of interest regarding the publication of this paper.

References

[1] The Hidden Technologies at the 2018 FIFA World Cup, June 4 2018. https://football-technology.fifa.com/en/blog/hidden-technologies-at-the-2018-fwc

[2] Laws of the Game-FIFA, 2015/2016. https://img.fifa.com/image/upload/datdz0pms85gbnqy4j3k.pdf

[3] VICON Motion Capture System. https://www.vicon.com/motion-capture

[4] Cortes, N., Blount, E., Ringleb, S. and Onate, J.A. (2011) Soccer-Specific Video Simulation for Improving Movement Assessment. *Sports Biomechanics*, **10**, 22-34. https://doi.org/10.1080/14763141.2010.547591

[5] Bodenheimer, B., Rose, C., Rosenthal, S. and Pella, J. (1997) The Process of Motion Capture: Dealing with the Data. In: *Computer Animation and Simulation*, Springer-Verlag, Berlin, 3-18. https://doi.org/10.1007/978-3-7091-6874-5_1

Call for Papers

World Journal of Mechanics (WJM)

ISSN 2160-049X (Print) ISSN 2160-0503 (Online)
http://www.scirp.org/journal/wjm

World Journal of Mechanics (WJM) is an international peer-reviewed journal dedicated to presenting the English original research studies, reviews in the general field of mechanics including the mechanics of solids, structures and fluids and their interaction.

Subject Coverage

This journal invites original research and review papers that address the following issues. Topics of interest include, but are not limited to:

- Applied Mathematics and Mechanics
- Biomechanics and Modeling in Mechanobiology
- Celestial Mechanics and Dynamical Astronomy
- Classical and Quantum Aspects of Mechanics
- Computational Mechanics
- Computer Methods in Applied Mechanics and Engineering
- Continuum Mechanics and Thermodynamics
- Damage Mechanics
- Dynamics and Vibration Control
- Elasticity and Plasticity
- Engineering Fracture Mechanics
- Environmental Fluid Mechanics
- Experimental Mechanics
- Fluid Mechanics and Aerodynamics
- Mathematical Fluid Mechanics
- Mathematics and Mechanics of Solids
- Mechanical Behavior of Biomedical Materials
- Mechanical Engineering Science
- Mechanical Systems and Signal Processing
- Mechanics & Astronomy
- Mechanics and Materials in Design
- Mechanics in Medicine and Biology
- Mechanics of Materials
- Mechanics of Time-Dependent Materials
- Microfluidics
- Micromechanics and Microengineering
- Multi-Scale Mechanics
- Nanomechanics
- Non-Linear Mechanics
- Non-Newtonian Fluid Mechanics
- Numerical and Analytical Methods in Geomechanics
- Probabilistic Engineering Mechanics
- Rock Mechanics and Mining Sciences
- Solid and Structural Mechanics
- Statistical Mechanics and Its Applications
- Terramechanics
- Theoretical and Applied Fracture Mechanics
- Thermophysics and Aeromechanics
- Thin Film Mechanics
- Viscoelasticity

We are also interested in short papers (letters) that clearly address a specific problem, and short survey or position papers that sketch the results or problems on a specific topic. Authors of selected short papers would be invited to write a regular paper on the same topic for future issues of World Journal of Mechanics.

Notes for Intending Authors

Submitted papers should not have been previously published nor be currently under consideration for publication elsewhere. Paper submission will be handled electronically through the website. All papers are refereed through a peer review process. For more details about the submissions, please access the website.

Website and E-Mail

http://www.scirp.org/journal/wjm E-mail: wjm@scirp.org

What is SCIRP?

Scientific Research Publishing (SCIRP) is one of the largest Open Access journal publishers. It is currently publishing more than 200 open access, online, peer-reviewed journals covering a wide range of academic disciplines. SCIRP serves the worldwide academic communities and contributes to the progress and application of science with its publication.

What is Open Access?

All original research papers published by SCIRP are made freely and permanently accessible online immediately upon publication. To be able to provide open access journals, SCIRP defrays operation costs from authors and subscription charges only for its printed version. Open access publishing allows an immediate, worldwide, barrier-free, open access to the full text of research papers, which is in the best interests of the scientific community.

- High visibility for maximum global exposure with open access publishing model
- Rigorous peer review of research papers
- Prompt faster publication with less cost
- Guaranteed targeted, multidisciplinary audience

Scientific Research Publishing

Website: http://www.scirp.org
Subscription: sub@scirp.org
Advertisement: service@scirp.org